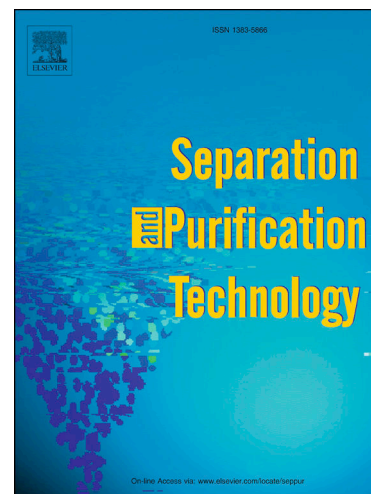


Journal Pre-proofs

Carbon black and polydopamine modified non-woven fabric enabling efficient solar steam generation towards seawater desalination and wastewater purification

Shuangjie Sun, Binbin Sun, Yameng Wang, Maxwell Fordjour Antwi-Afari, Hao-Yang Mi, Zhanhu Guo, Chuntai Liu, Changyu Shen

PII: S1383-5866(21)01329-0
DOI: <https://doi.org/10.1016/j.seppur.2021.119621>
Reference: SEPPUR 119621



To appear in: *Separation and Purification Technology*

Received Date: 23 June 2021
Revised Date: 11 August 2021
Accepted Date: 29 August 2021

Please cite this article as: S. Sun, B. Sun, Y. Wang, M. Fordjour Antwi-Afari, H-Y. Mi, Z. Guo, C. Liu, C. Shen, Carbon black and polydopamine modified non-woven fabric enabling efficient solar steam generation towards seawater desalination and wastewater purification, *Separation and Purification Technology* (2021), doi: <https://doi.org/10.1016/j.seppur.2021.119621>

This is a PDF file of an article that has undergone enhancements after acceptance, such as the addition of a cover page and metadata, and formatting for readability, but it is not yet the definitive version of record. This version will undergo additional copyediting, typesetting and review before it is published in its final form, but we are providing this version to give early visibility of the article. Please note that, during the production process, errors may be discovered which could affect the content, and all legal disclaimers that apply to the journal pertain.

© 2021 Published by Elsevier B.V.

Carbon black and polydopamine modified non-woven fabric enabling efficient solar steam generation towards seawater desalination and wastewater purification

Shuangjie Sun¹, Binbin Sun¹, Yameng Wang¹, Maxwell Fordjour Antwi-Afari³, Hao-Yang Mi^{1}, Zhanhu Guo^{2*}, Chuntai Liu¹, Changyu Shen¹*

¹ National Engineering Research Center for Advanced Polymer Processing Technology, The Key Laboratory of Advanced Materials Processing & Mold of Ministry of Education, Zhengzhou University, Zhengzhou 450001, PR China

² Integrated Composites Laboratory (ICL), Department of Chemical & Biomolecular Engineering, University of Tennessee, 1015 Volunteer Boulevard, Knoxville, Tennessee 37996, United States

³ Department of Civil Engineering, College of Engineering and Physical Sciences, Aston University, Birmingham, B4 7ET, United Kingdom

*Corresponding Author. Email: mihaoyang@zzu.edu.cn (H.Y. Mi)

*Corresponding Author. Email: zguo10@utk.edu (Z. Guo)

Declaration of Competing Interest:

The authors declare no competing financial interest.

Abstract

The utilization of solar energy for steam generation is a highly efficient and sustainable technology for seawater desalination to solve the long-standing water crisis. Carbon-based materials have shown promising thermal-heat conversion efficiency due to their broadband solar absorption. Herein, carbon black (CB) was combined with polydopamine (PDA) to develop a high-performance, low-cost, and scalable PDA/CB@PP composite non-woven fabric was fabricated by dip-coating of CB and in situ polymerization of PDA. The hierarchical structure constructed on the fiber surface and the synergetic effects of CB and PDA contributed to the high light absorbance (>95%), superhydrophilicity, and high energy conversion efficiency. The one-way fluidic PDA/CB@PP photothermal based solar steam evaporator demonstrated a high evaporation rate of $1.68 \text{ kg m}^{-2} \text{ h}^{-1}$ with a solar steam efficiency of 91.5%. Moreover, the PDA/CB@PP fabric shows remarkable salt resistance when purifying seawater because of the water channel preserved by the hydrophilic porous structure of the fabric which could provide sustained water supply. Besides, the PDA/CB@PP fabric possesses excellent purification capability to wastewaters contaminated by heavy-metal and chemical dyes. This study provides insights into the design and development of low-cost, scalable, highly stable, and efficient solar steam generators for seawater desalination and wastewater purification.

Keywords: solar steam generation, carbon black, polydopamine, salt resistance, desalination

1. Introduction

The shortage of readily available clean water is becoming a critical challenge for the development and maintenance of functioning societies, as the expanding of industrialization and urbanization [1-5]. Traditional methods, such as distillation, electrodialysis, and reverse osmosis, have been widely used to produce clean water [6-8]. However, serious environmental problems and energy consumption are common consequences of these techniques [9]. Sunlight as an environmentally friendly and sustainable natural energy has played an essential role in various fields from ancient times right up to the present day [10]. As one important way of utilizing solar energy, solar steam generation has emerged as a solar-thermal technology that can efficiently convert sunlight into heat to generate clean water from seawater and even industrial wastewater via photothermal materials [11-13]. Compared with traditional seawater purification technologies that typically require large plants and great energy consumption, such as reverse osmosis, solar steam generation evaporator potentially enables the design of home-scale solar steam generation devices, which utilize solar energy, at a fairly low cost [14-18].

An efficient photothermal material is the core of the solar steam generator. It serves as a heat generation unit that converts solar energy into thermal energy. [19-21] It also acts as an evaporation platform that utilizes thermal energy to generate steam. [22-25] Moreover, it needs to have excellent dynamic water transportation capability to maintain a continuous water supply on its surface and prevent crystallization of salt granules during the evaporation process. [26] Great efforts have been made by researchers to fulfill all these

requirements and improve the thermal-heat conversion efficiency and evaporation efficiency [27-31].

Various solar absorber materials, such as biomass-derived carbon materials, carbon-based materials, natural materials, synthetic polymers, plasmonic nanomaterials, black semiconductor materials, etc., have been employed to develop photothermal evaporators [25,26, 32-37]. Biomass-derived carbon materials, as a low-cost, stable, green, abundant, and sustainable alternative for solar steam generation, have attracted attention in the scientific community lately [33,38]. Tan et al. [32] reported a sustainable way of repurposing food waste that not only mitigates carbon emission but also turns food waste into highly porous biomass-derived carbon-based photothermal materials for low-cost solar desalination and thermoelectric generation with an energy conversion efficiency ~85% and power output of 0.4 Wm^{-2} . Carbon-based materials have been found to possess high solar energy conversion efficiency in the range of 50-90% due to their broadband solar absorption and also possess advantages of abundant resource and physicochemical stability. Li et al. [26] fabricated a solar steam generator by coating reduced graphene oxide on the surface of a blank hollow spacer fabric (BHSF) filled with chitosan, which reached an evaporation efficiency of 86% under one sun solar illumination. Hu et al. [37] designed a carbon nanotube (CNT)-coated cellulose nanofibrils (CNFs) aerogel solar steam generator for efficient solar utilization with a solar-energy conversion efficiency of 76.3% and $1.11 \text{ kg m}^{-2} \text{ h}^{-1}$ under one solar irradiation. Carbon black (CB) as a low-cost carbonaceous nanomaterial has extraordinary chemical stability and broadband solar absorption, which makes it ideal for the fabrication of a photothermal evaporator. However, the low dispersion ability and adhesion strength of CB make it difficult to be applied to a substrate

material. The hydrophobicity of CB also limits the water transportation on its surface [39,40].

Natural biopolymers have been used in solar steam generation systems to enhance water transportation from the bulk water to the evaporation surface [3,9,34]. Polydopamine (PDA), a melanin-based biopolymer, has broadband solar absorption, noble photothermal conversion efficiency, nontoxicity, biodegradability, and excellent hydrophilicity. PDA has also been used in the preparation of photothermal evaporators [3]. For instance, Song et al. [9] deposited PDA and silver nanoparticles (AgNPs) on natural wood to prepare a solar interface evaporation device which displayed a high absorbance. Li et al. [41] developed a PDA coated raw wood solar steam generator with a solar vapor generation efficiency of ~77% under one sun illumination. However, sole PDA coating is difficult to achieve high light absorbance, and it may take several days of treatment to reach high solar energy conversion efficiency [41,42].

The rational combination of CB and PDA is expected to result in a high-performance hybrid coating that integrates the high light absorbance advantage of CB and the superior hydrophilicity of PDA. Based on this conception, a facile dip-coating and in situ polymerization approach was proposed to fabricate a high-performance, low-cost, scalable PDA/CB@polypropylene (PP) composite non-woven fabric for solar steam generation. The CB nanoparticles constructed hierarchical structures on the PP fibers, and the PDA coating not only fastened the adhesion among CB nanoparticles and between CB to the PP fiber effectively but also transformed the hydrophobic fabric surface to superhydrophilic. The hierarchical porous structure of the PDA/CB@PP fabric facilitates the light reflection and scattering, and the synergetic effect of PDA and CB could promote light absorbance

effectively. The beneficial structural and material merits endowed the one-way fluidic PDA/CB@PP photothermal based solar steam evaporator with excellent light absorption (>95%) in a wide wavelength range (300-2500 nm), and a high evaporation rate of 1.68 kg m⁻² h⁻¹ with an 91.5% solar steam efficiency under one sun irradiation. In addition, the PDA/CB@PP-based solar steam evaporator showed extraordinary salt resistance and high efficiency when purifying seawater due to the water channel preserved by the porous structure and hydrophilicity of the fabric. It also demonstrated the ability to purify various wastewater contaminated by heavy-metal and chemical dyes.

2. Experimental

2.1. Materials

CB nanoparticles were purchased from Degussa (Printex-U). Ethanol, dioxane, dopamine hydrochloride, tris(hydroxymethyl)aminomethane, anhydrous ferric chloride, zinc chloride, strontium chloride hexahydrate, copper nitrate hydrate, sodium chloride, magnesium chloride, potassium chloride, calcium chloride, dichloromethane (DCM), methylene blue (MB), and methyl orange (MO) were purchased from Aladdin. PP non-woven fabric was bought from a local grocery shop. All the chemicals were used as received without further purification.

2.2. Fabrication of CB@PP non-woven fabric

PP non-woven fabric was cut into 2 cm × 2 cm with long strips (6 cm × 1 cm) on both sides, and washed in water by ultrasonication for 10 min, and then dried at 70 °C for 5 h before use. CB nanoparticles were dispersed in dioxane by ultrasonication for 1 h to form dispersion with a concentration of 5 mg/ml. Subsequently, PP non-woven was immersed

into the CB solution for 20 min at 40 °C followed by drying at 80 °C for 2 h, and the process was repeated one to three times.

2.3. Fabrication of PDA@PP and PDA/CB@PP non-woven fabric

Dopamine hydrochloride (6 mg/mL) and tris(hydroxymethyl)aminomethane (3.6 mg/ml) were dissolved in deionized water. PP non-woven and CB@PP samples were dipped in the solution followed by continuously stirring for 8 h at 800 rpm, during which PDA was polymerized on the non-woven fabric. The resulting PDA@PP and PDA/CB@PP non-woven fabrics were washed with deionized water at least five times and dried at room temperature for 24 h.

2.4. Material characterization

The morphologies of different samples were characterized by a field emission scanning electron microscope (SEM, Zeiss MERLIN Compact). The samples were sputtered with a thin film of gold before observation. The wettability of the relevant samples was investigated by water contact angle (WCA) measuring instrument (OCA-20, Data-physics) and a high-speed video camera (Photron, FASTCAM Mini AX200) at ambient temperature. The light absorption spectrum of the samples was measured using a UV-Vis-NIR spectrophotometer (ranging from 300-2500 nm) equipped with an integrating sphere (PerkinElmer, Lambda950). An infrared thermal imaging camera (E60, FLIR) was employed to record the surface temperature change of different samples.

2.5. Preparation and purification of simulated wastewater

Dye contaminated wastewater was prepared using 40 mg/L MB and 40 mg/L MO. The decoloration efficiency of organic dyes was measured by ultraviolet-visible-near infrared (UV-vis-NIR) spectrometer (PerkinElmer lambda 750S). Heavy-metal

contaminated wastewater was prepared by dissolving ZnCl_2 (~148 mg), $\text{SrCl}_2 \cdot 6\text{H}_2\text{O}$ (~93 mg), $\text{Cu}(\text{NO}_3)_2 \cdot 3\text{H}_2\text{O}$ (~68 mg), and $\text{FeCl}_3 \cdot 6\text{H}_2\text{O}$ (~125 mg) in 500 mL DI water followed by sufficient ultrasonication. The ion concentrations of the wastewater and the corresponding purified water were measured by PerkinElmer 8300 inductively coupled plasma optical emission spectrometer (ICP-OES) and PerkinElmer NexION 300X inductively coupled plasma mass spectrometer (ICP-MS).

2.6. Solar steam generation experiments

The solar steam generation tests were conducted via a lab-made online testing system consisted of a solar simulator (Xenon arc lamp, PE300L-3A, Ceaulight) equipped with a solar filter (AM 1.5, Ceaulight), an infrared camera (E60, FLIR), an electronic balance (JA5003B, Shanghai Yue Ping Scientific Instruments Manufacturing Co., Ltd.), an optical power meter (CEL-FZ-A, Ceaulight), and a wet and dry thermometer (ZG-8012, Chigo). The room temperature was kept at ~20 °C, and the relative humidity was balanced about 50%. Polystyrene foam of ~4 cm thickness was used as a thermal insulator and support, which was ditched with two slots about 0.5 cm width and 1 cm length, and the spatial distance between the two slots was 2 cm. The two strips of the photothermal absorber were threaded across the two slots and stretch into bulk water. Thus, the effective evaporation area of the solar steam generation system was about $2 \times 2 \text{ cm}^2$.

3. Results and discussion

The schematic illustration of the whole preparation process is shown in Fig. 1a. Besides the advantages of outstanding chemical resistance and low cost, the PP non-woven exhibited excellent water transport property, which can draw water to the evaporation surface in 240 s due to the capillary effect of the fibrous structure and hydrophilicity surface

(Fig. 1b and Fig. S1). The digital photograph and microstructure results indicated that the pristine PP non-woven fabric is comprised of fibers with a diameter of $\sim 20 \mu\text{m}$ (Fig. S2). The PP photothermal materials were prepared by sequential dip-coating in a CB solution and in situ polymerization with PDA on the surface. The PP fabric could be easily converted to a black non-woven fabric after dip-coating, and the CB coating could render the fabric broadband solar absorption ability. The in situ polymerized PDA layer could enhance to the stability of the coating and improve the surface hydrophilicity at the same time. Besides, the developed process is easy to be scaled up to fabricate CB/PDA@PP photothermal materials as large as $10 \text{ cm} \times 10 \text{ cm}$ (Fig. 1c), and all PDA/CB@PP samples possess excellent flexibility, which could be distorted into various shapes without disassociation of nanoparticles (Fig. S3).

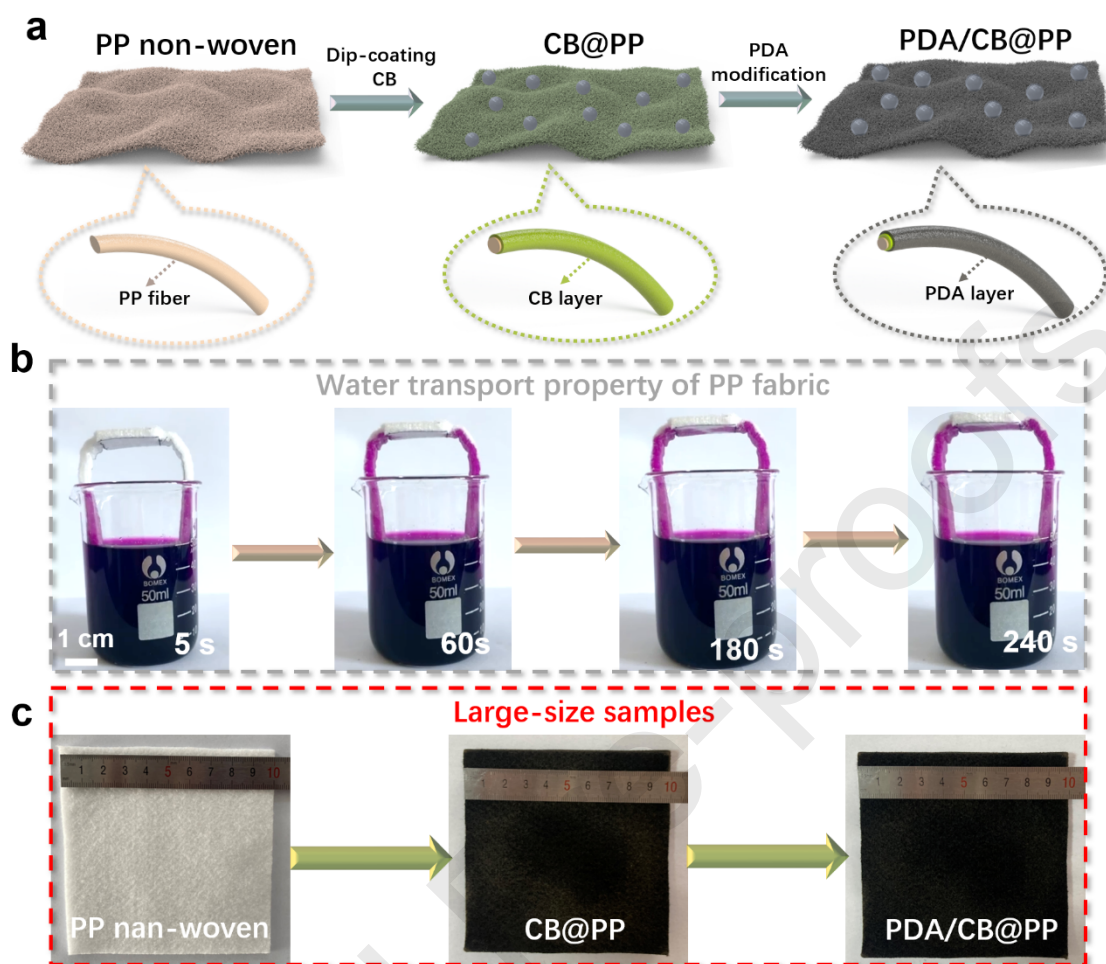


Fig. 1. (a) Schematic illustration of the preparation process of the PDA/CB@PP samples. (b) The water (dyed with KMnO_4) transport behavior of the PP non-woven fabric at different time points. (c) Digital images of large-size PP non-woven, CB@PP, and PDA/CB@PP samples.

The PP non-woven fabric was immersed into the CB solution followed by drying at 80°C , and the process was repeated one to three times, and relative samples were named as CB1@PP, CB2@PP, and CB3@PP, respectively. The CB in dioxane solution had a super dark color and could remain a homogenous suspension after 48 h (Fig. S4), suggesting high absorption capacity and stability. Fig. 2a₁-c₁ show the photographs of the CB1@PP, CB2@PP, and CB3@PP samples, respectively. It can be seen that the surface of non-woven fabrics became black after the deposition of CB, and the color was significantly darkened with the increase of dip-coating times. The SEM images revealed

the surface morphology of the samples. There were few CB granules dispersed on the surface of the CB1@PP sample (Fig. 2a₂-a₄), and the amount of CB significantly increased on the surface of the CB2@PP sample (Fig. 2b₂-b₄). The CB3@PP sample (Fig. 2c₂-c₄) displayed large CB clusters aggregated on its surface. These results confirmed that the concentration of CB on the surface of the PP non-woven fabric could be effectively enhanced by increasing coating times.

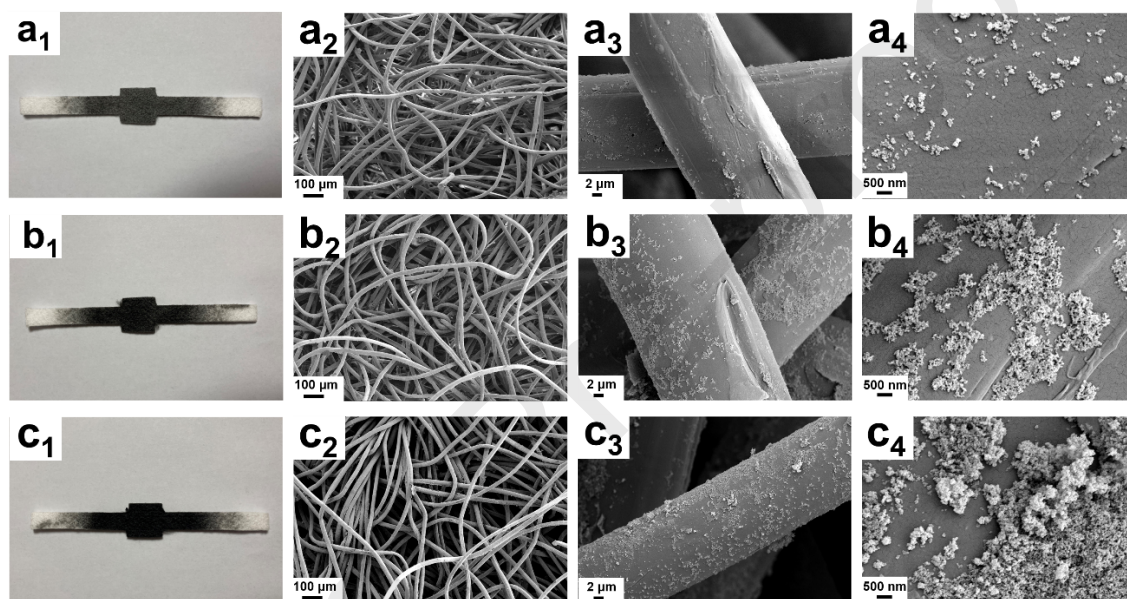


Fig. 2. Digital photographs of (a₁) CB1@PP, (b₁) CB2@PP, and (c₁) CB3@PP samples. SEM images of (a₂-a₄) CB1@PP, (b₂-b₄) CB2@PP, (c₂-c₄) CB3@PP surfaces at different magnifications.

Light absorption is a critical feature impacting solar steam generation. To quantify the light absorption properties of the CB@PP samples, light transmittance, reflection, and absorption spectrum characterizations were conducted using an UV-vis-NIR spectrophotometer equipped with an integrating sphere. The CB1@PP, CB2@PP, and CB3@PP all exhibited relatively low transmittances throughout the entirety solar spectrum (Fig. 3a), and the incident light irradiated on the CB2@PP and CB3@PP samples exhibited significantly lower reflection than the CB1@PP sample (Fig. 3b). The average absorption

from 300 nm to 2500 nm wavelength in the solar spectrum for the CB1@PP, CB2@PP, and CB3@PP samples were 76.8%, 91.2%, and 94.2%, respectively (Fig. 3c). The solar-thermal properties of the CB@PP photothermal materials were systematically examined. As shown in Fig. 3d, the surface temperature variations of CB1@PP, CB2@PP, and CB3@PP samples in a dry state under one sun illumination were recorded using an infrared thermal imaging camera. The light to heat performance can be quantified by the surface equilibrium temperature (T_c) of the samples. [4,43] It was observed that the surface temperatures of CB1@PP, CB2@PP, and CB3@PP all exhibited a rapid increase upon light irradiation, attributing to the good photothermal performance of the CB granules. A stable T_c of 74.3 °C was achieved within 360 s for the CB3@PP sample, whereas the corresponding T_c of CB1@PP and CB2@PP samples were 65.0 °C and 71.9 °C, respectively (Fig. 3d). The corresponding IR-thermal images at the initial state and the equilibrium state of different CB@PP samples were shown in Fig. 3e-g, indicating uniform heating of the photothermal materials under solar illumination. However, the WCA measurement results (Fig. 3h) indicated that all the CB@PP samples possess a WCA above 100°, which would make them hard to be fully wetted by the water, thus hindering the transportation of water molecules during solar steam generation.

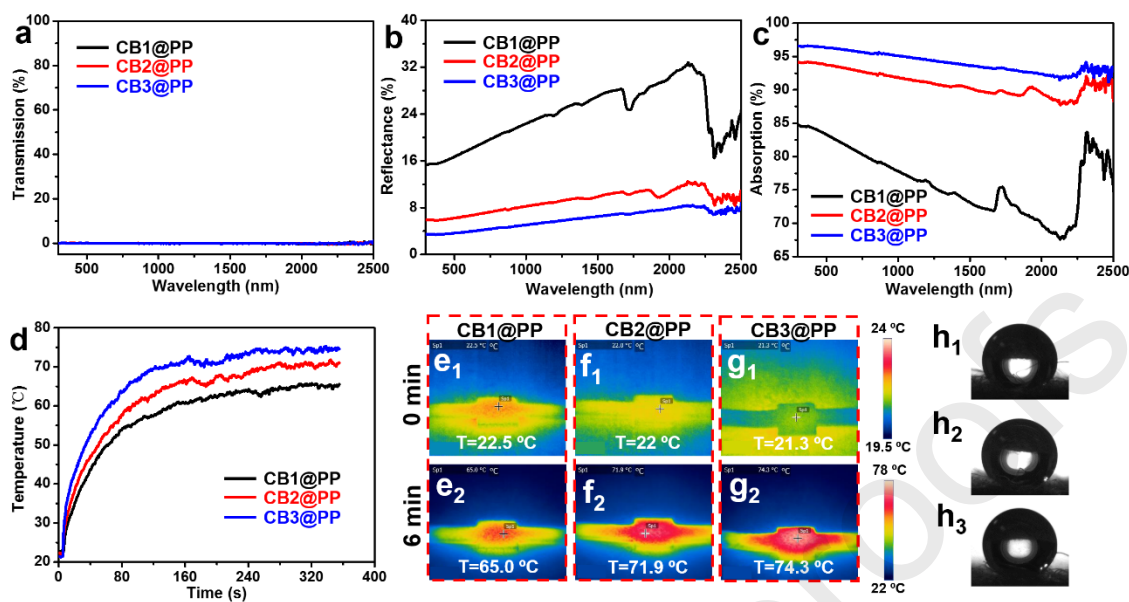


Fig. 3. (a) Reflectance (b) transmission, and (c) absorption spectra of CB1@PP, CB2@PP, and CB3@PP samples. (d) The temperature change of CB1@PP, CB2@PP, and CB3@PP samples under one sun solar illumination. Infrared images of (e₁, e₂) CB1@PP (f₁, f₂) CB2@PP, and (g₁, g₂) CB3@PP surfaces at the initial state and the equilibrium state. Surface wettability of (h₁) CB1@PP, (h₂) CB2@PP, and (h₃) CB3@PP samples.

To transform the wettability of CB@PP samples and study the synergistic effect of CB and PDA, the PP non-woven fabric, CB1@PP, CB2@PP, and CB3@PP samples, were coated with PDA via in situ dopamine polymerization process. The resulted samples were denoted as PDA@PP, PDA/CB1@PP, PDA/CB2@PP, and PDA/CB3@PP, respectively. Corresponding photographs were shown as Fig. 4a₁-d₁, and the change of surface morphology was investigated via SEM and energy dispersive spectroscopy (EDS) mapping. It was found that the PDA coating layer formed thin films covering the PP fiber. The EDS mapping analysis of PDA@PP samples are displayed in Fig. S5a₁-a₂, and the table in Figure S5a₁ shows the proportion of C and N elements, which were 70% and 30%, respectively. The N element was ascribed to the PDA and it was distributed homogeneously on the surface of the fiber, which proved even distribution of PDA on the fiber. However, cracking of the PDA coating layer was observed on the PDA@PP (Fig.

4a₂-a₄) and PDA/CB1@PP (Fig. 4b₂-b₄) samples, which may be caused by the internal stress in the continuous PDA film during the drying process. The thickness of the PDA layer depends on the self-polymerization time, and it was ~20 nm on the surface of nanoparticles when in situ polymerization on fabric for 8 h. [36]. The cracking phenomena were absent for the PDA/CB2@PP (Fig. 4c₂-c₄) and PDA/CB3@PP (Fig. 4d₂-d₄) samples, which suggested that the internal stress of PDA coating was dissipated by the CB nanoparticles. As shown in the table of Fig. S5b₁-d₁, the proportion of C and N changed as the increase of CB. The amount of C was increased from 74% to 82%, and the N was decreased from 26% to 18%, due to the increased CB deposition. In addition, the N element was uniformly distributed along the fibers (Fig. S5b-d), indicating that the CB particles are homogeneously covered with PDA layer. In addition, the PDA coating obviously enhanced the bonding among the CB nanoparticles and tightly packed the coating materials on the PP fibers, which should be favorable for improving the stability of the coating layer.

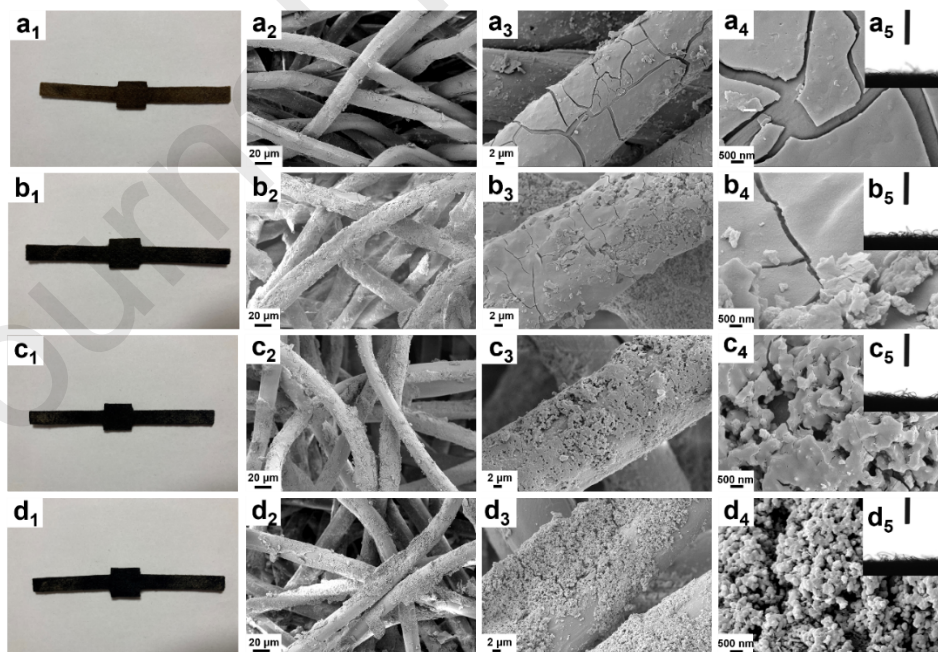


Fig. 4. Digital photographs of (a₁) PDA@PP, (b₁) PDA/CB1@PP, (c₁) PDA/CB2@PP, and (d₁) PDA/CB3@PP samples. SEM images of (a₂-a₄) PDA@PP, (b₂-b₄) PDA/CB1@PP,

(c₂-c₄) PDA/CB2@PP, and (d₂-d₄) PDA/CB3@PP samples at different magnifications. Surface wettability of (a₅) PDA@PP, (b₅) PDA/CB1@PP, (c₅) PDA/CB2@PP, and (d₅) PDA/CB3@PP samples.

The WCA measurement results indicated that all samples had been effectively transformed to superhydrophilic after PDA coating, as shown in Fig. 4a₅-d₅. The water transportation and absorption performance of the PDA-coated samples were investigated in detail. It was found that the water could be efficiently drawn and spread across the entire surface of PDA@PP, PDA/CB1@PP, PDA/CB2@PP, and PDA/CB3@PP samples in 40 s, 60 s, 95 s, and 110 s, respectively, as indicated by the change of surface temperature recorded using an IR camera (Fig. 5a). The water absorption performance was evaluated by recording the absorption process of a water droplet on the sample surface (Fig. 5b). The trend of water absorption was the same as the water transportation tests, and the water droplet could be rapidly absorbed by the photothermal materials within 63.5 ms. The faster water absorption and transportation rate of PDA@PP than the PDA/CB@PP was because of the hierarchical nanostructure presented on the surface of PDA/CB@PP sample, which prevented the infiltration of water into the voids among fibers. The hydrophilic surface of PDA/CB@PP is favorable for water transportation, and the relatively slow transportation rate could facilitate the evaporation surface to maintain high temperature and evaporation efficiency.

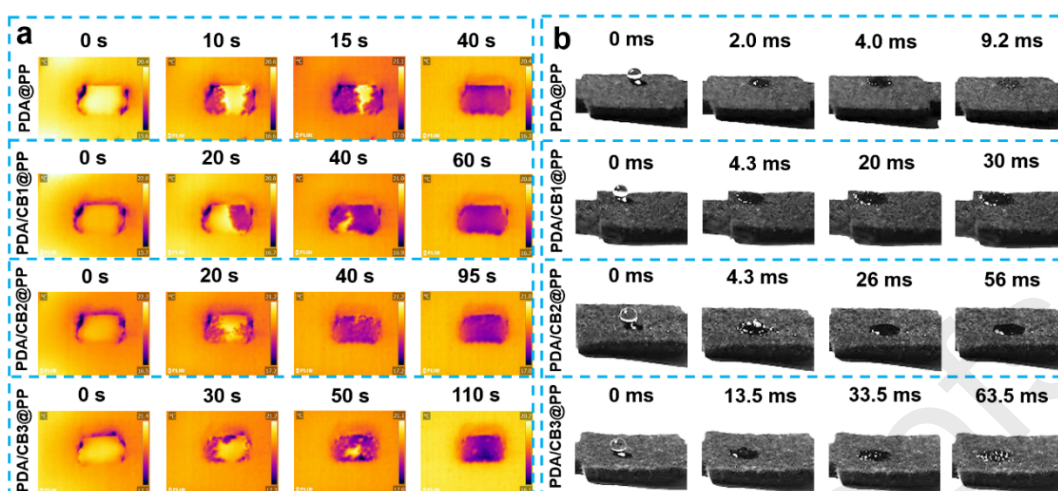


Fig. 5. (a) Water transportation behavior of the PDA@PP, PDA/CB1@PP, PDA/CB2@PP, and PDA/CB3@PP samples indicated by the spreading of the wetted area over time recorded by an infrared camera. (b) The absorption process of a water droplet placed on the surfaces of PDA@PP, PDA/CB1@PP, PDA/CB2@PP, and PDA/CB3@PP recorded using a high-speed video camera.

The light absorption properties of PDA-coated samples were characterized as well. It was found that the transmittances of all samples were about zero in the entire solar spectrum (Fig. 6a). The reflectance (Fig. 6b) and absorption (Fig. 6c) spectra showed that the introduction of a PDA coating layer could further enhance the average absorption of PDA/CB1@PP, PDA/CB2@PP, and PDA/CB3@PP samples to 89.8%, 93.4%, and 95.2%, respectively. However, the PDA@PP sample had a relatively low average absorption rate of 62.5%, which suggested the synergetic effect of CB and PDA in improving the solar absorbance. The solar irradiation experiments (Fig. 6d) showed that the equilibrium T_c of PDA@PP, PDA/CB1@PP, PDA/CB2@PP, and PDA/CB3@PP samples were 67.6 °C, 70.6 °C, 73.4 °C, and 75.5 °C, respectively, which is in agreement with the results obtained in the light absorption experiments. The T_c of PDA coated samples were generally higher than the corresponding CB@PP samples. According to the literature [44], the absorptivity value of PDA/CB3@PP is 0.81, and theoretical analyses and calculation of the absorptivity value is provided in the Supporting Information. In addition, the surfaces of the

PDA/CB@PP samples were uniformly heated under solar illumination (Fig. 6e-h), demonstrating outstanding photothermal property.

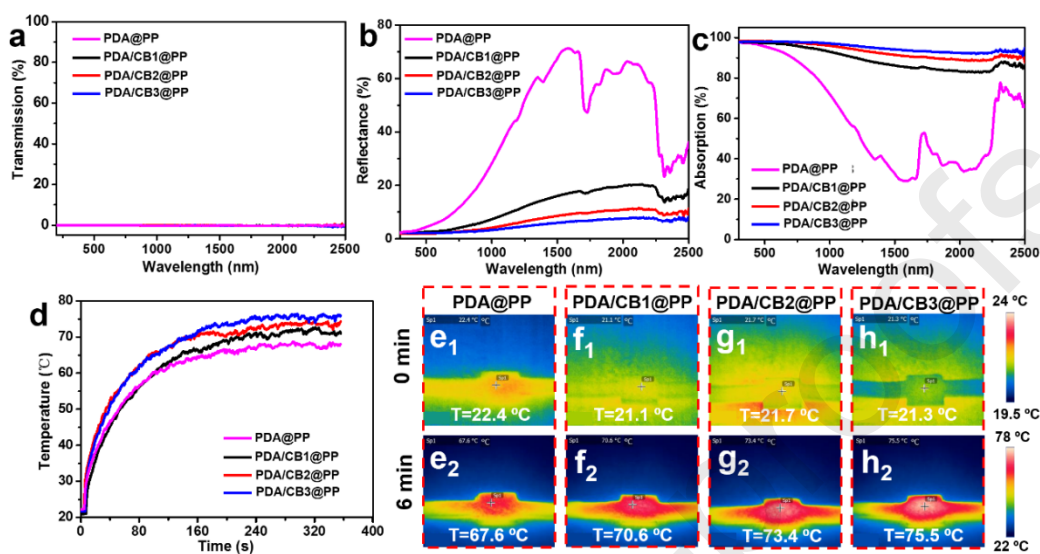


Fig. 6. (a) Reflectance (b) transmission, and (c) absorption spectra of PDA@PP, PDA/CB1@PP, PDA/CB2@PP, and PDA/CB3@PP samples. (d) The temperature change of PDA@PP, PDA/CB1@PP, PDA/CB2@PP, and PDA/CB3@PP samples under one sun solar illumination. Infrared images of (e₁, e₂) PDA@PP (f₁, f₂) PDA/CB1@PP, (g₁, g₂) PDA/CB2@PP, and (h₁, h₂) PDA/CB3@PP surfaces at the initial state and the equilibrium state.

Solar steam generation experiments were carried out using a lab-made, real-time measurement system (Fig. 7a), which is equipped with a solar simulator, computer, infrared camera, and electronic balance. A polystyrene (PS) foam was placed between the photothermal material and the water to prevent heat loss. Fig. 7b and c show the infrared photographs of the surface temperature change for the PDA coated PP fabric and CB@PP fabrics when illuminated with one sun under wet condition and their corresponding temperature profiles. The maximum temperature of the PDA@PP was 39.5 °C within 15 min, while the surface temperature of PDA/CB1@PP, PDA/CB2@PP, and PDA/CB3@PP reached 40.6 °C, 41.3 °C, and 42.0 °C within 15 min under one sun illumination. The evaporation efficiency of solar generators is indicated by the mass change of bulk water

under the solar illumination of one sun. It was found that the mass change of all samples had a linear function over time (Fig. 7d), and their corresponding water evaporation rates were calculated from the slope of the linear curves. The evaporation rate for PDA@PP was only $1.21 \text{ kg m}^{-2} \text{ h}^{-1}$, while it was $1.29 \text{ kg m}^{-2} \text{ h}^{-1}$, $1.36 \text{ kg m}^{-1} \text{ h}^{-1}$, and $1.41 \text{ kg m}^{-2} \text{ h}^{-1}$ for the PDA/CB1@PP, PDA/CB2@PP, and PDA/CB3@PP samples, respectively (Fig. 7e), indicating dramatic improvement when the CB was combined with PDA in the coating layer. Theoretical analyses of heat loss [45] and the calculation of energy conversion efficiency of the PDA/CB3@PP evaporator are provided in the Supporting Information. The evaporation efficiency of PDA coated PP fabric and CB@PP fabrics were calculated to 64.8%, 70.4%, 75.3%, and 78.8%, respectively, under one sun irradiation (detailed calculation shown in Supporting Information) [46-48]. Therefore, the evaporation efficiency of the optimum solar steam generator, PDA/CB3@PP, was 14 % higher than the PDA@PP sample without CB. The excellent solar evaporation performance of the PDA/CB3@PP was attributed to the light scattering and the synergistic effect between the CB nanoparticles and the PDA coating layer [49]. As illustrated in Fig. 7f, the hierarchical structures constructed on the fiber surface of PDA/CB3@PP are highly favorable for light scattering, and the porous structure of the fabric could result in the light reflection inside the material and facilitate light absorbance at the same time [50,51]. Besides, the synergetic effect of PDA and CB could promote the light absorbance greatly [52], and the thermal heat generated could be effectively transferred throughout the evaporation surface by the hybridized CB nanoparticles due to their high intrinsic thermal conductivity [53], which lead to the localized heating of the PDA/CB3@PP surface and a high maximum surface temperature. Moreover, the PS foam located beneath the PDA/CB3@PP provided

excellent thermal insulation property, which effectively reduced the heat loss of the solar evaporation system.

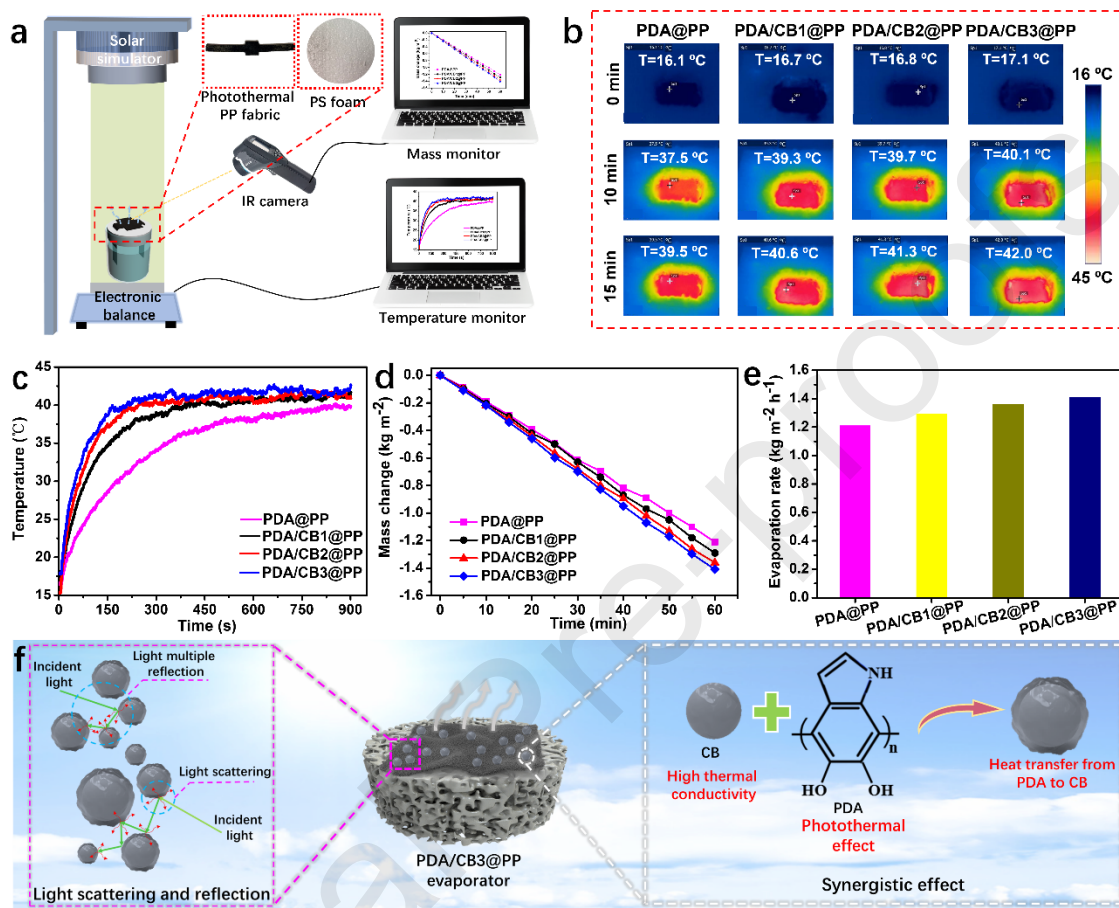


Fig. 7. (a) Schematic illustration of the solar steam generation device equipped with a solar simulator, electrical balance, and an infrared thermal imaging camera. (b) Infrared images of PDA@PP, PDA/CB1@PP, PDA/CB2@PP, and PDA/CB3@PP drawing water at different time intervals under one sun irradiation. (c) The temperature change of PDA@PP, PDA/CB1@PP, PDA/CB2@PP, and PDA/CB3@PP sample under one sun illumination when drawing water. (d, e) Mass change and evaporation rate of PDA@PP, PDA/CB1@PP, PDA/CB2@PP, and PDA/CB3@PP in pure water under one sun irradiation. (f) Schematic of solar steam generation mechanism for the solar evaporator based on the PDA/CB3@PP.

Salt crystallization and accumulation on the surface of solar steam generators is a critical issue that limits their long-term performance [54,55]. The desalination performance of the developed PDA/CB3@PP evaporator was investigated using real seawater collected

from the Yellow Sea of China. The experiment was conducted in a simulated natural environment under one sun irradiation for 10 h illumination. As shown in Fig. 8a, the corresponding evaporation rate remained about $1.4 \text{ kg m}^{-2} \text{ h}^{-1}$ during the continuous evaporation process, and no salt crystals were observed as indicated by the inset photographs. To further investigate the salt resistance behavior of the PDA/CB3@PP evaporator, solid NaCl granules were placed on top of it during the continuous evaporation process of seawater (Figure 8b), the corresponding evaporation rate was shown in Figure S7. It was found that the added salt granules could be gradually dissolved and eventually disappeared on the surface of the PDA/CB3@PP in ~ 3.5 h. As the dissolving of salt particles, the evaporation rate was gradually increased. These results demonstrated the outstanding salt-rejection ability of the PDA/CB3@PP, which was mainly attributed to the following two reasons. First, the salt concentration difference created by the evaporation process triggered the diffusion and convection of salt ions and water molecules in the strips connecting to the bulk water due to the 3.7 times water content of the PDA/CB3@PP evaporator, which facilitated the transportation of salt ions to the bulk water (Fig. 8c) [56]. Second, the loosely porous structure and interconnected water channels of the hydrophilic PDA/CB3@PP make it able to rapidly pump and replenish the surface vaporized seawater (Fig. 8d) [19]. Hence, the developed PDA/CB3@PP evaporator could not only prevent salt crystallization, but also re-dissolve salt granules on its surface.

Water is transported from the bulk water to the photothermal layer in the solar steam generation system and evaporated on it. As shown in Figure 8e, the specific weight of developed evaporators in the dry and wet states was tested. It is evident that the evaporation rate and efficiency of the conventional CB3/PDA@PP are higher than the other three

conventional evaporators, and the water content of the conventional PDA/CB3@PP evaporator was 3.7 g g^{-1} . The excess water content on the conventional PDA/CB3@PP evaporator would waste the solar heat and limit the contact area between the water and the air, which would result in a limited evaporation rate [57,58]. To further enhance the evaporation rate and efficiency of the CB3/PDA@PP absorber, a one-way fluidic photothermal system was assembled (Fig. 8f and Fig. S8), which is composed of a water-wicking single-layer microfiber non-woven fabric (MNF) inlet with a width of 2 cm, a PDA/CB3@PP absorber, and a wicking double-layer MNF outlet with a width of 3 cm. During the solar evaporation process, bulk water was wicked from a saline reservoir to the PDA/CB3@PP absorber via the inlet, and the evaporated fluid is discharged through the outlet (Fig. 8g and Fig. S9) [28,59,60]. Single-layer and double-layer MNF were employed for water transportation to reduce the water content of the one-way PDA/CB3@PP absorber (Fig. 8f). When the one-way fluidic photothermal system was used, the water evaporation rate of the PDA/CB3@PP was $1.68 \text{ kg m}^{-2} \text{ h}^{-1}$ with a solar steam efficiency of 91.5% under one sun solar radiation (Fig. 8h), which is 12.7% higher than the conventional PDA/CB3@PP evaporator. The one-way PDA/CB3@PP evaporator had the lowest real-time water content (Fig. 8e), which leads to minimal heat exchange between the solar absorber and the water [59]. Therefore, the evaporation rate of the fluidic photothermal system is the highest. Moreover, the evaporation rate of one-way PDA/CB3@PP was maintained around $1.68 \text{ kg m}^{-2} \text{ h}^{-1}$ (Fig. 8i) during 5 h under one sun solar radiation, indicating high evaporation stability of the fluidic photothermal system. A continuous fresh water generation setup was assembled to collect pure water using the PDA/CB3@PP photothermal evaporator (Fig. S10). Over 3.15 g of water was collected within 5 h

illumination using one-way fluidic PDA/CB@PP photothermal evaporator (about 7.8 cm-2 in projected area).

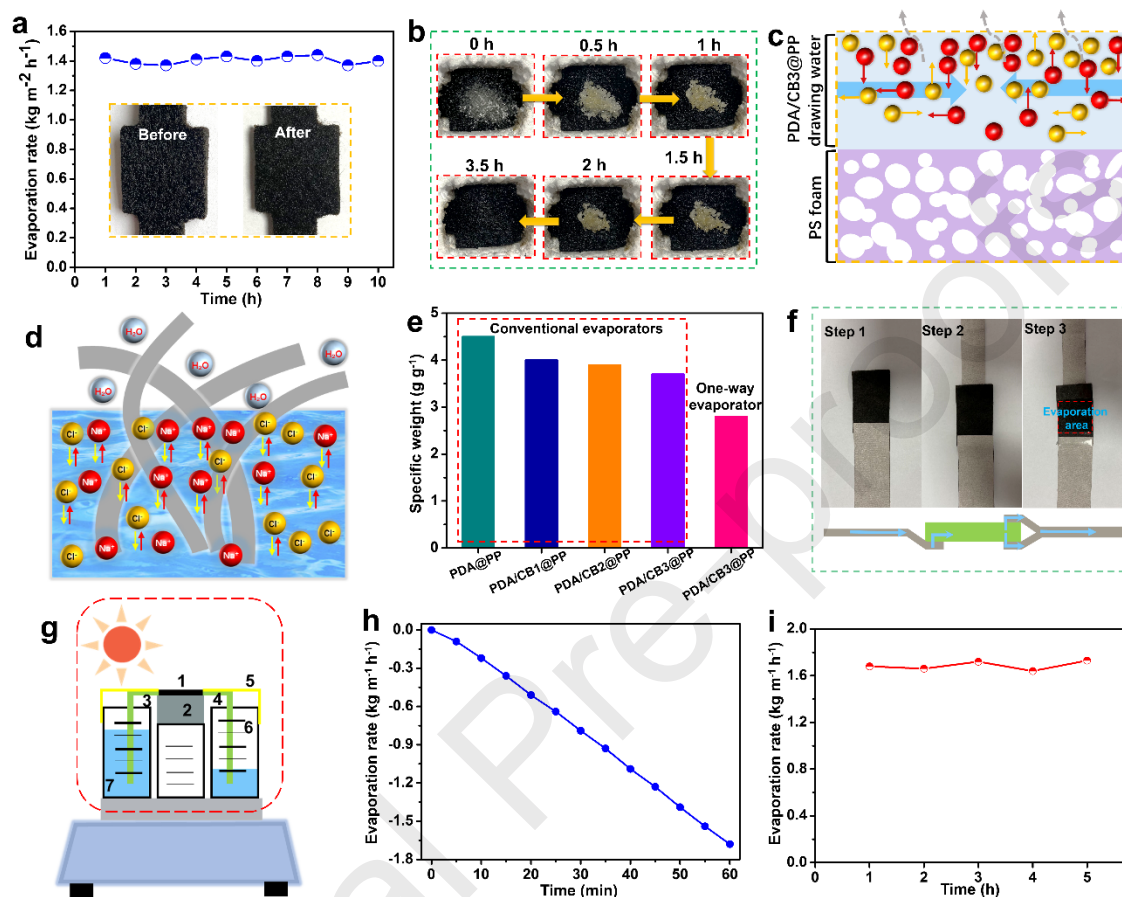


Fig. 8. (a) Evaporation rate of the conventional PDA/CB3@PP when drawing seawater for 10 h under one sun illumination; Inset photographs show the surface of conventional PDA/CB3@PP before and after 10 h continuous operation drawing seawater. (b) Digital pictures of a salt rejection progression of the PDA/CB3@PP under solar illumination of one sun. (c) Schematics of the transport path of water and salt ions on the evaporation surface of PDA/CB3@PP. (d) Illustration of the salt dissolution process of PDA/CB3@PP evaporator during solar desalination. (e) The specific weight of the developed evaporator in wet and dry states. (f) Digital photographs and water transportation mechanism of the one-way PDA/CB3@PP fluidic photothermal system. (g) Schematic of the experimental setup for quantitative solar evaporation evaluation. The numbers represent (1) solar absorber, (2) PS foam, (3) inlet, (4) outlet, (5) reflective cover, (6) discharge, and (7) seawater reservoir. (h) Mass change of one-way PDA/CB3@PP evaporator under one sun irradiation. (i) Evaporation rate of the one-way fluidic PDA/CB3@PP evaporator for 5 h under one sun illumination.

To analyze the desalination performance of the PDA/CB3@PP based evaporator, the steam generated was gathered using a transparent polypropylene film (Fig. S11), and the concentration of ions was evaluated using an ICP-OES. The concentrations of four primary ions (Ca^{2+} , K^+ , Mg^{2+} , and Na^+) in the seawater before and after desalination were shown in Fig. 9a, from which it is clear that the concentration of all ions was decreased by two to three orders of magnitude, and was significantly lower than the safe salinity levels defined by standards set by the World Health Organization (WHO) and the US Environmental Protection Agency (EPA). In addition, the electrical resistance measurement results indicated that the resistance of seawater was enhanced from 17.7 k Ω to 0.41 M Ω when purified via the PDA/CB3@PP based evaporator (Fig. S12). The resistance of the purified water was even higher than that of domestic water (0.31 M Ω), suggesting successful desalination of seawater into high-quality freshwater.

The purification performance of the PDA/CB3@PP based evaporator to various wastewaters was further investigated to demonstrate their practical applicability. The purification performance to heavy-metal contaminated wastewater containing Cu^{2+} , Fe^{3+} , Sr^{2+} , and Zn^{2+} was evaluated by measuring the ion concentration using an ICP-MS. As shown in Fig. 9b, the ion concentrations of the condensate water were significantly decreased with ion rejection rate beyond 99.9%. The electrical resistances of the wastewater and purified water were 2.39 k Ω and 0.35 M Ω respectively (Fig. S12), suggesting high purification efficiency. The UV-vis spectrum of heavy-metal contaminated wastewater was measured before and after purification, which showed that the absorption peak was disappeared completely after purification (Fig. 9c).

Moreover, the PDA/CB3@PP based evaporator was also used to purify wastewaters containing methylene blue (MB) and methyl orange (MO), respectively. As shown in Fig. 9d, the MB contaminated water changed from blue to transparent, and all absorption peaks in the UV-vis spectrum were disappeared after purification, indicating that the MB has been effectively eliminated from the water. Similarly, the PDA/CB3@PP based evaporator also exhibit excellent performance in purifying MO contaminated water as indicated by the UV-vis spectrum (Fig. 9e). Therefore, the PDA/CB3@PP holds prominent potential for heavy metal ions removal and wastewater purification processes.

In addition, the cost-effectiveness (ε) should be concerned for practical clean water production. The cost of the developed one-way fluidic photothermal PDA/CB3@PP evaporator was estimated to be ~ 33.37 \$ m⁻² (Table S1), which is much lower than the evaporators based on graphene and MXene [61-63]. The cost-effectiveness can be calculated by equation (1) [64]

$$\varepsilon = r/c \quad (1)$$

Where r refers to evaporation rate (kg m⁻² h⁻¹) and c is the materials cost (\$ m⁻²). It was found that the PDA/CB3@PP had high cost-effectiveness of 50.3 g h⁻¹ \$⁻¹, which outperformed majority of recently reported solar evaporators (Fig. 9f) [65-70]. Therefore, the PDA/CB3@PP evaporator developed in this study is highly cost-effective and possesses excellent evaporation efficiency, self-desalting capacity, and wastewater purification properties, making it an ideal candidate material for practical desalination or freshwater production.

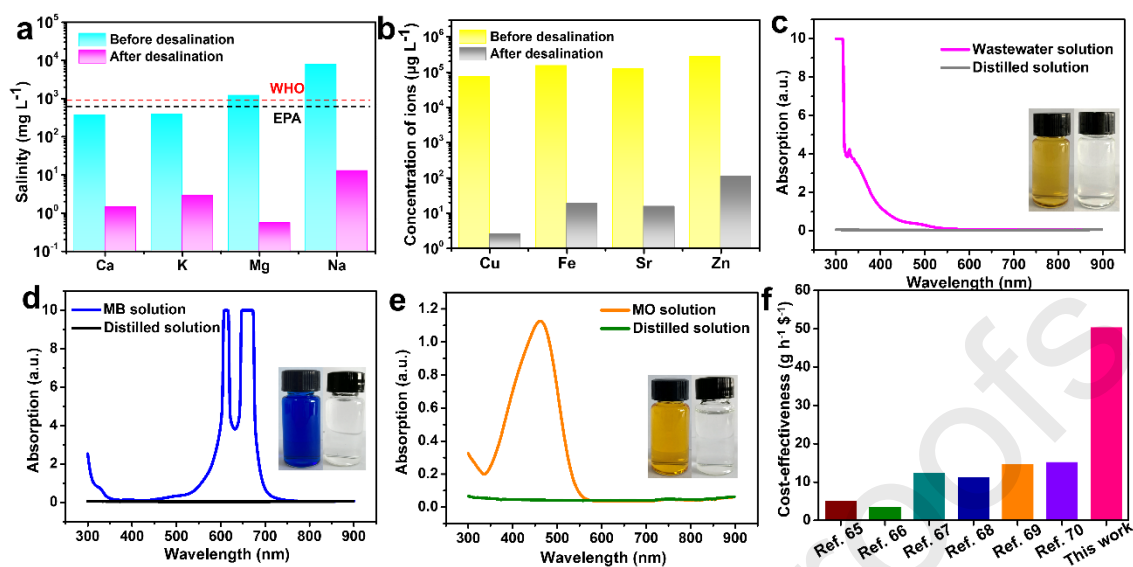


Fig. 9. (a) Salinity values of the metal ions before and after purification. (b) Concentrations of the heavy metal ions in the wastewater before and after purification. UV-vis absorption spectra of (c) wastewater, (d) MB, and (e) MO solutions before evaporation and corresponding purified waters after evaporation; Insert photographs show the color change after purification. (f) Comparison of cost-effectiveness between this work and relevant literature.

4. Conclusions

In this study, an efficient solar steam evaporator was prepared by depositing CB and PDA on PP non-woven fabric. The coating of CB nanoparticles resulted in a high equilibrium surface temperature of 74.3 °C under one sun illumination. The introduction of PDA coating further enhanced the surface temperature to 75.5 °C and rendered the fabric with superhydrophilicity. The optimum one-way fluidic PDA/CB@PP photothermal evaporator achieved a high evaporation rate of 1.68 kg m⁻² h⁻¹ under one sun and a corresponding evaporation efficiency of approximately 91.5%, attributing to the hierarchical structures constructed by the CB nanoparticles and PDA coating, and the synergetic effects of the CB and PDA. The PDA/CB3@PP evaporator possesses excellent salt resistance over 10 h of continuous operation in seawater desalination and the ion concentration of the purified seawater was reduced by 2 to 3 order of magnitudes. The

porous structure and hydrophilic nature of the PDA/CB3@PP facilitated rapid water pumping, which replenishes the water on the evaporating surface and prevents salt accumulation. Moreover, the PDA/CB3@PP evaporator demonstrated superior performance in the purification of wastewater contaminated by heavy-metal and chemical dyes. Finally, the finding of this study may provide new inspiration for the design and development of highly stable, high efficiency, low-cost, and scalable solar steam generators for seawater desalination and wastewater purification.

Conflict of interest

The authors declare no competing financial interest.

Acknowledgements

This work was supported by the National Natural Science Foundation of China (51603075, 12072325), National Key R&D Program of China (2019YFA0706802).

References

- [1] L. Zhou, Y. Tan, J. Wang, W. Xu, Y. Yuan, W. Cai, J. Zhu, 3D self-assembly of aluminium nanoparticles for plasmon-enhanced solar desalination, *Nat. Photonics* 10 (2016) 393-398.
- [2] P. Mu, L. Song, L. Geng, J. Li, Aligned Attapulgite-based aerogels with excellent mechanical property for the highly efficient solar steam generation, *Sep. Purif. Technol.* 271 (2021) 118869.
- [3] X. Xu, S. Ozden, N. Bizmark, C.B. Arnold, S.S. Datta, R.D. Priestley, A Bioinspired Elastic Hydrogel for Solar - Driven Water Purification, *Adv. Mater.* 33 (2021) 2007833.

- [4] X. Fan, Y. Yang, X. Shi, Y. Liu, H. Li, J. Liang, Y. Chen, A MXene-Based Hierarchical Design Enabling Highly Efficient and Stable Solar-Water Desalination with Good Salt Resistance, *Adv. Funct. Mater.* 30 (2020) 2007110.
- [5] Y. Zhu, D. Joralmon, W. Shan, Y. Chen, J. Rong, H. Zhao, S. Xiao, X. Li, 3D printing biomimetic materials and structures for biomedical applications, *Bio-Des. Manuf.* 4 (2021) 405-428.
- [6] M.J. Earle, J.M. Esperança, M.A. Gilea, J.N.C. Lopes, L.P. Rebelo, J.W. Magee, J.A. Widegren, The distillation and volatility of ionic liquids, *Nature* 439 (2006) 831-834.
- [7] J. Wiśniewski, A. Róžańska, Donnan dialysis with anion-exchange membranes as a pretreatment step before electrodialytic desalination, *Desalination* 191 (2006) 210-218.
- [8] L. Gong, C. Li, N. Wei, J. Li, J. Shen, R. Xu, H. Cui, Highly Efficient Solar Evaporator Based on Graphene/MoO_{3-x} Coated Porous Nickel for Water Purification, *Sep. Purif. Technol.* 275 (2021) 119139.
- [9] J. Yang, Y. Chen, X. Jia, Y. Li, S. Wang, H. Song, Wood-Based Solar Interface Evaporation Device with Self-Desalting and High Antibacterial Activity for Efficient Solar Steam Generation, *ACS Appl. Mater. Interfaces* 12 (2020) 47029-47037.
- [10] A. Zhang, W. Zheng, Z. Yuan, J. Tian, L. Yue, R. Zheng, J. Liu, Hierarchical NiMn-layered double hydroxides@ CuO core-shell heterostructure in-situ generated on Cu (OH)₂ nanorod arrays for high performance supercapacitors, *Chem. Eng. J.* 380 (2020) 122486.
- [11] J. Jia, W. Liang, H. Sun, Z. Zhu, C. Wang, A. Li, Fabrication of bilayered attapulgite for solar steam generation with high conversion efficiency. *Chem. Eng. J.* 361(2019) 999-1006.

- [12] Y. Xu, D. Liu, H. Xiang, S. Ren, Z. Zhu, D. Liu, H. Xu, F. Cui, W. Wang, Easily scaled-up photo-thermal membrane with structure-dependent auto-cleaning feature for high-efficient solar desalination, *J. Membrane Sci.* 586 (2019) 222-230.
- [13] H. Jian, Q. Qi, W. Wang, D. Yu, A Janus porous carbon nanotubes/poly (vinyl alcohol) composite evaporator for efficient solar-driven interfacial water evaporation, *Sep. Purif. Technol.* 264 (2021) 118459.
- [14] L. Zhao, L. Wang, J. Shi, X. Hou, Q. Wang, Y. Zhang, Y. Wang, N. Bai, J. Yang, J. Zhang, B. Yu, C.F. Guo, Shape-Programmable Interfacial Solar Evaporator with Salt-Precipitation Monitoring Function, *ACS Nano* 15 (2021) 5752-5761.
- [15] C. Wen, H. Guo, J. Yang, Q. Li, X. Zhang, X. Sui, M. Cao, L. Zhang, Zwitterionic hydrogel coated superhydrophilic hierarchical antifouling floater enables unimpeded interfacial steam generation and multi-contamination resistance in complex conditions. *Chem. Eng. J.* 421 (2021) 130344.
- [16] Z. Wang, M. Han, F. He, S. Peng, S.B. Darling, Y. Li, Versatile coating with multifunctional performance for solar steam generation, *Nano Energy* 74 (2020) 104886.
- [17] Z. Huang, S. Li, X. Cui, Y. Wan, Y. Xiao, S. Tian, C.S. Lee, A broadband aggregation-independent plasmonic absorber for highly efficient solar steam generation, *J. Mater. Chem. A* 8 (2020) 10742-10746.
- [18] T. Chen, Z. Wu, Z. Liu, J.T. Aladejana, X. Wang, M. Niu, Q. Wei, Y. Xie, Hierarchical porous aluminophosphate-treated wood for high-efficiency solar steam generation, *ACS Appl. Mater. Interfaces* 12 (2020) 19511-19518.
- [19] J. He, Z. Zhang, C. Xiao, F. Liu, H. Sun, Z. Zhu, W. Liang, A. Li, High-performance

- salt-rejecting and cost-effective superhydrophilic porous monolithic polymer foam for solar steam generation, *ACS Appl. Mater. Interfaces* 12 (2020) 16308-16318.
- [20] J. Li, X. Zhou, J. Zhang, C. Liu, F. Wang, Y. Zhao, H. Sun, Z. Zhu, W. Liang, A. Li, Migration crystallization device based on biomass photothermal materials for efficient salt-rejection solar steam generation, *ACS Appl. Energ. Mater.* 3 (2020) 3024-3032.
- [21] H. Wang, C. Zhang, Z. Zhang, B. Zhou, J. Shen, A. Du, Artificial Trees Inspired by *Monstera* for Highly Efficient Solar Steam Generation in Both Normal and Weak Light Environments, *Adv. Funct. Mater.* 30 (2020) 2005513.
- [22] J. He, Y. Fan, C. Xiao, F. Liu, H. Sun, Z. Zhu, W. Liang, A. Li, Enhanced solar steam generation of hydrogel composite with aligned channel and shape memory behavior, *Compos. Sci. Technol.* 204 (2021) 108633.
- [23] X. Shan, A. Zhao, Y. Lin, Y. Hu, Y. Di, C. Liu, Z. Gan, Low-Cost, Scalable, and Reusable Photothermal Layers for Highly Efficient Solar Steam Generation and Versatile Energy Conversion, *Adv. Sustain. Syst.* 4 (2020) 1900153.
- [24] C. Kim, Y. Ryu, D. Shin, A.M. Urbas, K. Kim, Efficient solar steam generation by using metal-versatile hierarchical nanostructures for nickel and gold with aerogel insulator, *Appl. Surf. Sci.* 517 (2020) 146177.
- [25] J. Chen, B. Li, G. Hu, R. Aleisa, S. Lei, F. Yang, D. Liu, F. Lyu, M. Wang, X. Ge, F. Qian, Q. Zhang, Y. Yin, Integrated Evaporator for Efficient Solar-Driven Interfacial Steam Generation, *Nano Lett.* 20 (2020) 6051-6058.
- [26] F. Wang, D. Wei, Y. Li, T. Chen, P. Mu, H. Sun, Z. Zhu, W. Liang, A. Li, Chitosan/reduced graphene oxide-modified spacer fabric as a salt-resistant solar

- absorber for efficient solar steam generation, *J. Mater. Chem. A* 7 (2019) 18311-18317.
- [27] A. Elbaz, Z. He, B. Gao, J. Chi, E. Su, D. Zhang, S. Liu, H. Xu, H. Liu, Z. Gu, Recent biomedical applications of bio-sourced materials, *Bio-Des. Manuf.* 1 (2018) 26-44.
- [28] Y. Zhang, T. Xiong, D.K. Nandakumar, S.C. Tan, Structure Architecting for Salt-Rejecting Solar Interfacial Desalination to Achieve High-Performance Evaporation with in Situ Energy Generation, *Adv. Sci.* 7 (2020) 1903478.
- [29] X. Li, D. Wang, Y. Zhang, L. Liu, W. Wang, Surface-ligand protected reduction on plasmonic tuning of one-dimensional MoO_{3-x} nanobelts for solar steam generation, *Nano Res.* 13 (2020) 3025-3032.
- [30] B. Bai, X. Yang, R. Tian, X. Wang, H. Wang, A high efficiency solar steam generation system with using residual heat to enhance steam escape, *Desalination* 491 (2020) 114382.
- [31] H. Jiang, H. Fang, D. Wang, J. Sun, Spray-coated commercial PTFE membrane from $\text{MoS}_2/\text{LaF}_3/\text{PDMS}$ ink as solar absorber for efficient solar steam generation, *Sol. RRL* 4 (2020) 2000126.
- [32] Y. Zhang, S.K. Ravi, S.C. Tan, Food-derived carbonaceous materials for solar desalination and thermo-electric power generation, *Nano Energy* 65 (2019) 104006.
- [33] Y. Zhang, S.K. Ravi, J.V. Vaghasiya, S.C. Tan, A barbeque-analog route to carbonize moldy bread for efficient steam generation, *iScience* 3 (2018) 31-39.
- [34] Q. Jiang, H.G. Derami, D. Ghim, S. Cao, Y.S. Jun, S. Singamaneni, Polydopamine-filled bacterial nanocellulose as a biodegradable interfacial photothermal evaporator for highly efficient solar steam generation, *J. Mater. Chem. A* 5 (2017) 18397-18402.

- [35] P. Mu, Z. Zhang, W. Bai, J. He, H. Sun, Z. Zhu, W. Liang, A. Li, Superwetting monolithic hollow-carbon-nanotubes aerogels with hierarchically nanoporous structure for efficient solar steam generation, *Adv. Energy Mater.* 9 (2019) 1802158.
- [36] H. Moon, Y.C. Lee, J. Hur, One-pot decoration of cupric oxide on activated carbon fibers mediated by polydopamine for bacterial growth inhibition, *Materials* 13 (2020) 1158.
- [37] F. Jiang, H. Liu, Y. Li, Y. Kuang, X. Xu, C. Chen, H. Huang, C. Jia, X. Zhao, E. Hitz, Y. Zhou, R. Yang, L. Cui, L. Hu, Lightweight, mesoporous, and highly absorptive all-nanofiber aerogel for efficient solar steam generation, *ACS Appl. Mater. Interfaces* 10 (2018) 1104-1112.
- [38] H.M. Wilson, D.J. Ahirrao, S.R. Ar, N. Jha, Biomass-derived porous carbon for excellent low intensity solar steam generation and seawater desalination, *Sol. Energ. Mat. Sol. C.* 215 (2020) 110604.
- [39] M. Sansotera, C.L. Bianchi, G. Lecardi, G. Marchionni, P. Metrangolo, G. Resnati, W. Navarrini, Highly hydrophobic carbon black obtained by covalent linkage of perfluorocarbon and perfluoropolyether chains on the carbon surface, *Chem. Mater.* 21 (2009) 4498-4504.
- [40] Y. Chen, L. Wang, Z. Wu, J. Luo, B. Li, X. Huang, H. Xue, J. Gao, Super-hydrophobic, durable and cost-effective carbon black/rubber composites for high performance strain sensors, *Compos. Part B-Eng.* 176 (2019) 107358.
- [41] Y. Zou, P. Yang, L. Yang, N. Li, G. Duan, X. Liu, Y. Li, Boosting solar steam generation by photothermal enhanced polydopamine/wood composites, *Polymer* 2179 (2021) 123464.

- [42] Y. Yang, Y. Cheng, F. Deng, L. Shen, Z. Zhao, S. Peng, C. Shuai, A bifunctional bone scaffold combines osteogenesis and antibacterial activity via in situ grown hydroxyapatite and silver nanoparticles, *Bio-Des. Manuf.* (2021) 1-17.
- [43] K. Li, T.H. Chang, Z. Li, H. Yang, F. Fu, T. Li, J. Ho, P.Y. Chen, Light-to-heat conversion: biomimetic MXene textures with enhanced light-to-heat conversion for solar steam generation and wearable thermal management, *Adv. Energy Mater.* 9 (2019) 1970141.
- [44] K. Bae, B.J. Ku, Y. Kim, A. Mnoyan, K. Lee, K.J. Lee, Black diatom colloids toward efficient photothermal converters for solar-to-steam generation, *ACS Appl. Mater. Interfaces* 11 (2019) 4531-4540.
- [45] K. Go, K. Bae, H. Choi, H.Y. Kim, K.J. Lee, Solar-to-steam generation via porous black membranes with tailored pore structures, *ACS Appl. Mater. Interfaces* 11 (2019) 48300-48308.
- [46] Z. Liu, H. Song, D. Ji, C. Li, A. Cheney, Y. Liu, N. Zhang, B. Chen, J. Gao, Y. Li, X. Liu, D. Aga, S. Jiang, Z. Yu, Q. Gan, Extremely cost-effective and efficient solar vapor generation under nonconcentrated illumination using thermally isolated black paper, *Global Challenges* 1 (2017) 1600003.
- [47] M. Gao, C.K. Peh, H.T. Phan, L. Zhu, G.W. Ho, Solar absorber gel: Localized Macro-nano heat channeling for efficient plasmonic Au nanoflowers photothermic vaporization and triboelectric generation, *Adv. Energy Mater.* 8 (2018) 1870114.
- [48] K. Wang, B. Huo, F. Liu, Y. Zheng, M. Zhang, L. Cui, J. Liu, In situ generation of carbonized polyaniline nanowires on thermally-treated and electrochemically-etched carbon fiber cloth for high efficient solar seawater desalination, *Desalination* 481

(2020) 114303.

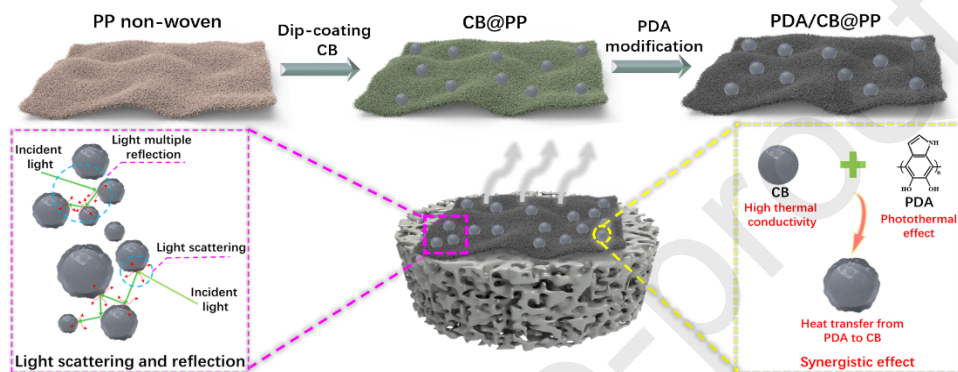
- [49] M. Chen, Y. Wu, W. Song, Y. Mo, X. Lin, Q. He, B. Guo, Plasmonic nanoparticle-embedded poly (p-phenylene benzobisoxazole) nanofibrous composite films for solar steam generation, *Nanoscale* 10 (2018) 6186-6193.
- [50] L.A. Weinstein, W.C. Hsu, S. Yerci, S.V. Boriskina, G. Chen, Enhanced absorption of thin-film photovoltaic cells using an optical cavity, *J. Opt.* 17 (2015) 055901.
- [51] Q. Fang, T. Li, H. Lin, R. Jiang, F. Liu, Highly efficient solar steam generation from activated carbon fiber cloth with matching water supply and durable fouling resistance, *ACS Appl. Energ. Mater.* 2 (2019) 4354-4361.
- [52] X. Fan, Y. Ding, Y. Liu, J. Liang, Y. Chen, Plasmonic $Ti_3C_2T_x$ MXene enables highly efficient photothermal conversion for healable and transparent wearable device, *ACS Nano* 13 (2019) 8124-8134.
- [53] X. Wang, Y. Zhao, J. Jin, M. Song, A comparative study on the effect of carbon fillers on electrical and thermal conductivity of a cyanate ester resin, *Polym. Test.* 60 (2017) 293-298.
- [54] K. Liu, W. Zhang, H. Cheng, L. Luo, B. Wang, Z. Mao, X. Sui, X. Feng, A nature-inspired monolithic integrated cellulose aerogel-based evaporator for efficient solar desalination, *ACS Appl. Mater. Interfaces* 13 (2021) 10612-10622.
- [55] Y. Xia, Q. Hou, H. Jubaer, Y. Li, Y. Kang, S. Yuan, H. Liu, M.W. Woo, L. Zhang, L. Gao, H. Wang, X. Zhang, Spatially isolating salt crystallisation from water evaporation for continuous solar steam generation and salt harvesting, *Energy Environ. Sci.* 12 (2019) 1840-1847.
- [56] Y. Fan, W. Bai, P. Mu, Y. Su, Z. Zhu, H. Sun, W. Liang, A. Li, Conductively

- monolithic polypyrrole 3-D porous architecture with micron-sized channels as superior salt-resistant solar steam generators, *Sol. Energ. Mat. Sol. C.* 206 (2020) 110347.
- [57] Y. Zhang, S.K. Ravi, L. Yang, J.V. Vaghasiya, L. Suresh, I. Tan, S.C. Tan, Portable trilayer photothermal structure for hybrid energy harvesting and synergic water purification, *ACS Appl. Mater. Interfaces* 11 (2019) 38674-38682.
- [58] H. Liang, Q. Liao, N. Chen, Y. Liang, G. Lv, P. Zhang, B. Lu, L. Qu, Thermal efficiency of solar steam generation approaching 100% through capillary water transport, *Angew. Chem. Int. Edit.* 58 (2019) 19041-19046.
- [59] Y. Zhang, T. Xiong, L. Suresh, H. Qu, X. Zhang, Q. Zhang, J. Yang, S.C. Tan, Guaranteeing complete salt rejection by channeling saline water through fluidic photothermal structure toward synergistic zero energy clean water production and in situ energy generation, *ACS Energy Lett.* 5 (2020) 3397-3404.
- [60] Y. Zhang, H. Zhang, T. Xiong, H. Qu, J.J. Koh, D.K. Nandakumar, J. Wang, S.C. Tan, Manipulating unidirectional fluid transportation to drive sustainable solar water extraction and brine-drenching induced energy generation, *Energ. Environ. Sci.* 13 (2020) 4891-4902.
- [61] X. Zhao, X.J. Zha, J.H. Pu, L. Bai, R.Y. Bao, Z.Y. Liu, M.B. Yang, W. Yang, Macroporous three-dimensional MXene architectures for highly efficient solar steam generation, *J. Mater. Chem. A* 7 (2019) 10446-10455.
- [62] Z. Yu, P. Wu, Biomimetic MXene-polyvinyl alcohol composite hydrogel with vertically aligned channels for highly efficient solar steam generation, *Adv. Mater. Technol-US* 5 (2020) 2000065.

- [63] W. Li, X. Li, W. Chang, J. Wu, P. Liu, J. Wang, Vertically aligned reduced graphene oxide/Ti₃C₂T_x MXene hybrid hydrogel for highly efficient solar steam generation, *Nano Res.* 13 (2020) 3048-3056.
- [64] Y. Guo, H. Lu, F. Zhao, X. Zhou, W. Shi, G. Yu, Biomass-derived hybrid hydrogel evaporators for cost-effective solar water purification, *Adv. Mater.* 32 (2020) 1907061.
- [65] Q. Ma, P. Yin, M. Zhao, Z. Luo, Y. Huang, Q. He, Y. Yu, Z. Liu, Z. Hu, B. Chen, H. Zhang, MOF-based hierarchical structures for solar-thermal clean water production, *Adv. Mater.* 31 (2019) 1808249.
- [66] C. Chang, P. Tao, J. Xu, B. Fu, C. Song, J. Wu, W. Shang, T. Deng, High-efficiency superheated steam generation for portable sterilization under ambient pressure and low solar flux, *ACS Appl. Mater. Interfaces* 11 (2019) 18466-18474.
- [67] Y. Guo, X. Zhou, F. Zhao, J. Bae, B. Rosenberger, G. Yu, Synergistic energy nanoconfinement and water activation in hydrogels for efficient solar water desalination, *ACS Nano* 13 (2019) 7913-7919.
- [68] M. Zhu, Y. Li, G. Chen, F. Jiang, Z. Yang, X. Luo, Y. Wang, S.D. Lacey, J. Dai, C. Wang, C. Jia, J. Wan, Y. Yao, A. Gong, S. Das, L. Hu Tree-inspired design for high-efficiency water extraction, *Adv. Mater.* 29 (2017) 1704107.
- [69] L. Li, J. Zhang, Highly salt-resistant and all-weather solar-driven interfacial evaporators with photothermal and electrothermal effects based on Janus graphene@silicone sponges, *Nano Energy* 81 (2021) 105682.
- [70] X. Wang, Q. Liu, S. Wu, B. Xu, H. Xu, Multilayer polypyrrole nanosheets with self-organized surface structures for flexible and efficient solar-thermal energy conversion,

Adv. Mater. 31 (2019) 1807716.

Graphical Abstract



CRedit authorship contribution statement

Shuangjie Sun: Performing experiments, writing (original draft, and editing), data curation, visualization, formal analysis. **Binbin Sun:** Instruments, formal analysis, visualization. **Yameng Wang:** Formal analysis, conceptualization. **Maxwell Fordjour Antwi-Afari:** writing-reviewing, visualization. **Haoyang Mi:** Writing-reviewing, funding acquisition validation, conceptualization. **Zhanhu Guo:** methodology, writing-reviewing, formal analysis. **Chuntai Liu:** Project administration, funding acquisition. **Changyu Shen:** Project administration, funding acquisition.

Declaration of interests

The authors declare that they have no known competing financial interests or personal relationships that could have appeared to influence the work reported in this paper.

The authors declare the following financial interests/personal relationships which may be considered as potential competing interests:

Highlights

1. PDA/CB composite non-woven PP fabric was prepared for solar energy harvesting.
2. Hierarchical structure and synergetic effects of CB/PDA contributed to high light absorbance.
3. The evaporation rate of $1.68 \text{ kg m}^{-2} \text{ h}^{-1}$ with a solar steam efficiency of 91.5% was achieved.
4. The solar evaporator demonstrated superior salt resistance and ability to purify seawater and various wastewaters with high efficiency.